OPEN ACCESS Freely available online

PLOS ONE

Thermal and Concentration Stratifications Effects in Radiative Flow of Jeffrey Fluid over a Stretching Sheet

T. Hayat[1,2], Tariq Hussain[3], S. A. Shehzad[4]*, A. Alsaedi[2]

1 Department of Mathematics, Quaid-i-Azam University, Islamabad, Pakistan, **2** Nonlinear Analysis and Applied Mathematics (NAAM) Research Group, Department of Mathematics, Faculty of Science, King Abdulaziz University, Jeddah, Saudi Arabia, **3** Department of Mathematics, Faculty of Computing, Mohammad Ali Jinnah University, Islamabad Campus, Islamabad, Pakistan, **4** Department of Mathematics, Comsats Institute of Information Technology, Sahiwal, Pakistan

Abstract

In this article we investigate the heat and mass transfer analysis in mixed convective radiative flow of Jeffrey fluid over a moving surface. The effects of thermal and concentration stratifications are also taken into consideration. Rosseland's approximations are utilized for thermal radiation. The nonlinear boundary layer partial differential equations are converted into nonlinear ordinary differential equations via suitable dimensionless variables. The solutions of nonlinear ordinary differential equations are developed by homotopic procedure. Convergence of homotopic solutions is examined graphically and numerically. Graphical results of dimensionless velocity, temperature and concentration are presented and discussed in detail. Values of the skin-friction coefficient, the local Nusselt and the local Sherwood numbers are analyzed numerically. Temperature and concentration profiles are decreased when the values of thermal and concentration stratifications parameters increase. Larger values of radiation parameter lead to the higher temperature and thicker thermal boundary layer thickness.

Citation: Hayat T, Hussain T, Shehzad SA, Alsaedi A (2014) Thermal and Concentration Stratifications Effects in Radiative Flow of Jeffrey Fluid over a Stretching Sheet. PLoS ONE 9(10): e107858. doi:10.1371/journal.pone.0107858

Editor: Yinping Zhang, Tsinghua University, China

Received July 9, 2014; **Accepted** August 14, 2014; **Published** October 2, 2014

Data Availability: The authors confirm that all data underlying the findings are fully available without restriction. All relevant data are included within the paper.

Funding: This project is funded by the Deanship of Scientific Research (DSR) King Abdulaziz University, Jeddah, Saudi Arabia under grant no. 78-130-35-HiCi. The authors, therefore, acknowledge with thanks DSR. The funders had no role in study design, data collection and analysis, decision to publish, or preparation of the manuscript.

Competing Interests: The authors have declared that no competing interests exist.

* Email: s.a.shehzad@hotmail.com

Introduction

The boundary layer flow of non-Newtonian fluids gains a special attention of the researchers because of its wide occurrence in the industrial and engineering processes. The most commonly involved fluids in industry and technology are categorized as non-Newtonian. Many of the materials used in biological sciences, chemical and petroleum industries, geophysics etc. are also known as the non-Newtonian fluids. The non-Newtonian fluids are further divided into three main classes namely differential, rate and integral types. The simplest subclass of non-Newtonian fluids is the rate type fluids. The present study involves the Jeffrey fluid model which falls into the category of rate type non-Newtonian fluids. This fluid model exhibits the properties of ratio of relaxation to retardation times and retardation time. This model is very popular amongst the investigators. Few studies regarding Jeffrey fluid model are mentioned in the references [1–5].

The better cooling rate in the manufacturing processes is very essential for the best quality final product. For such processes, a controlled cooling system is required. An electrically polymeric liquid seems to be a good candidate for such applications of polymer and metallurgy because here the flow can be controlled by an applied magnetic field. Further the magnetohydrodynamic (MHD) flows are quite prominent in MHD power generating systems, cooling of nuclear reactors, plasma studies, geothermal energy extraction and many others. Interesting investigations on MHD flows can be seen in the references [6–11]. The thermal radiation effects have pivotal role in the industrial and engineering processes. Such processes are performed at very high temperature under various non-isothermal conditions and in situations where convective heat transfer coefficients are smaller. The radiative heat transfer can be used in hypersonic flights, model of pertinent equipment, nuclear power plants, nuclear reactors, gas turbines, space vehicles etc. [12–15].

Influence of stratification is an important aspect in heat and mass transfer analysis. The formation or deposition of the layers is known as the stratification. This phenomenon occurs due to the change in temperature or concentration, or variations in both, or presence of various fluids or different densities. It is quite important and interesting to examine the effects of combined stratifications (thermal and concentration stratifications) in mixed convective flow past a surface when heat and mass transfer analysis is performed simultaneously. Investigation of doubly stratified flows is a subject of special attention nowadays because of its broad range of applications in industrial and engineering processes. Few practical examples of these applications include heat rejection into the environment such as rivers, seas and lakes, thermal energy storage systems like solar ponds, mixture in industrial, food and manufacturing processing, density stratification of the atmosphere etc. Having all such applications in view, Hayat et al. [16] provided an analysis to examine the thermal stratification effects in mixed convective flow of Maxwell fluid over a stretching surface. Simultaneous effects of thermal stratification and thermal

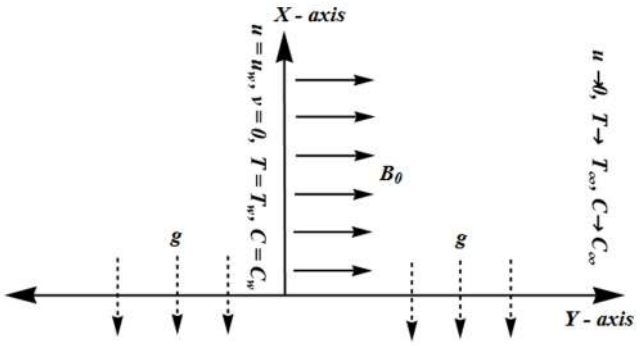

Figure 1. Physical model.
doi:10.1371/journal.pone.0107858.g001

radiation in stretched flow of thixotropic fluid are discussed by Shehzad et al. [17]. Ibrahim and Makinde [18] considered the effects of double stratifications in mixed convection flow of nanofluid past a vertical plate. Srinivasacharya and Upender [19] investigated the doubly stratified flow of micropolar fluid in the presence of an applied magnetic field. Soret and Dufour effects on doubly stratified flow of viscous fluid in a porous medium are studied by Srinivasacharya and Surender [20].

Here our main theme is to study the influences of thermal and concentration stratifications in mixed convection flow of Jeffrey fluid over a stretching sheet. Heat and mass transfer characteristics are encountered. Further, we considered the thermal radiation effect. Mathematical modelling is presented subject to boundary layer assumptions and Roseland's approximation. The governing nonlinear flow model is solved and homotopic solutions [21–35] of dimensionless velocity, temperature and concentration are presented. Physical quantities for various parameters of interest are examined. To our knowledge such analysis is not yet reported.

Governing Problems

We consider the mixed convection flow of an incompressible Jeffrey fluid over a stretching surface. Thermal and concentration stratifications are taken into account in the presence of thermal radiation. The vertical surface has temperature T_w and concentration C_w and further T_∞ and C_∞ are the temperature and concentration of ambient fluid. The x and $y-$ axes are chosen along and normal to the surface. The magnetic field of strength B_0 is applied normal to the flow direction (see Fig. 1). The effects of induced magnetic field are neglected due to the low magnetic Reynolds number. The governing partial differential equations under boundary layer assumptions are given below [4,14]:

$$\frac{\partial u}{\partial x}+\frac{\partial v}{\partial y}=0, \tag{1}$$

$$u\frac{\partial u}{\partial x}+v\frac{\partial u}{\partial y}= \frac{\nu}{1+\lambda_1}\left(\frac{\partial^2 u}{\partial y^2}+\lambda_2\left(\frac{\partial u}{\partial y}\frac{\partial^2 u}{\partial x\partial y}+u\frac{\partial^3 u}{\partial x\partial y^2}-\frac{\partial u}{\partial x}\frac{\partial^2 u}{\partial y^2}+v\frac{\partial^3 u}{\partial y^3}\right)\right) -\frac{\sigma B_0^2}{\rho}u+g\beta_T((T-T_\infty)+\beta_C(C-C_\infty)), \tag{2}$$

$$\rho C_p\left(u\frac{\partial T}{\partial x}+v\frac{\partial T}{\partial y}\right)=k\frac{\partial^2 T}{\partial y^2}-\frac{\partial q_r}{\partial y}, \tag{3}$$

$$u\frac{\partial C}{\partial x}+v\frac{\partial C}{\partial y}=D\frac{\partial^2 C}{\partial y^2}, \tag{4}$$

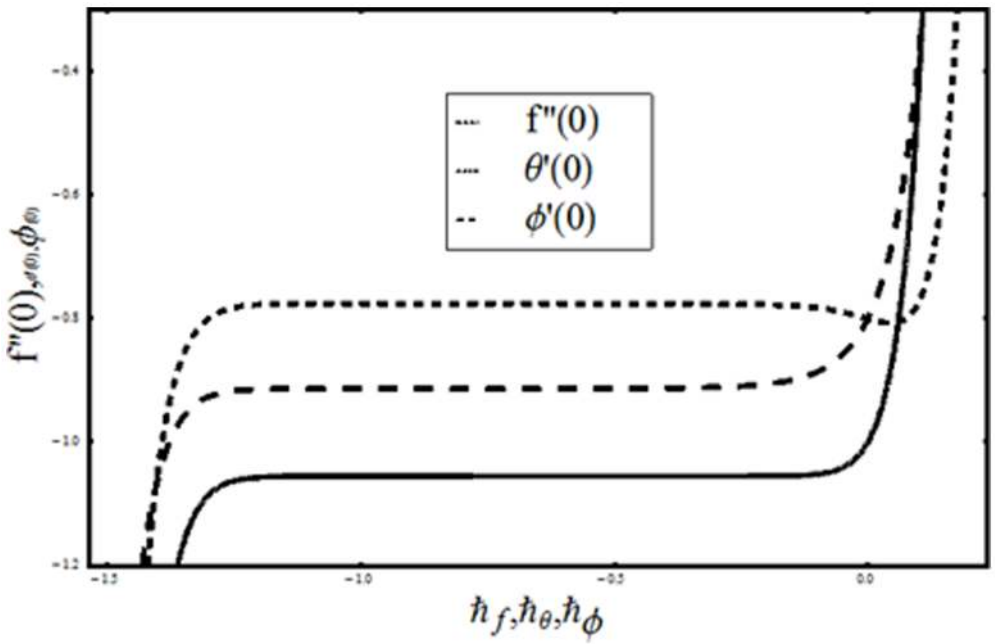

Figure 2. $\hbar-$ curves of functions $f(\eta)$, $\theta(\eta)$ and $\phi(\eta)$ at 17th-order of deformations when $M=0.6$, $\beta=0.4=Rd$, $\lambda_1=0.5$, $\lambda=0.3=N$, $\Pr=1.2$, $S=0.2=S^*$, $Sc=1.0$.
doi:10.1371/journal.pone.0107858.g002

Table 1. Convergence of homotopy solution for different order of approximations when $M=0.6$, $\beta=0.4=Rd$, $\lambda_1=0.5$, $\lambda=0.3=N$, Pr $=1.2$, $S=0.2=S^*$, $Sc=1.0$ and $\hbar_f=-0.7=\hbar_\theta=\hbar_\phi$.

Order of approximation	$-f''(0)$	$-\theta'(0)$	$-\phi'(0)$
01	1.060200	0.790667	0.870000
10	1.055105	0.776083	0.913029
17	1.055116	0.776004	0.913502
24	1.055118	0.775996	0.913543
28	1.055118	0.775996	0.913547
35	1.055118	0.775996	0.913547
40	1.055118	0.775996	0.913547

where u and v denote the velocity components in the $x-$ and $y-$ directions, ρ the fluid density, λ_1 the ratio of relaxation to retardation times, λ_2 the retardation time, g the gravitational acceleration, β_T the thermal expansion coefficient, β_C the concentration expansion coefficient, C_p the specific heat at constant pressure, T the fluid temperature, k the thermal conductivity of fluid, q_r the radiative heat flux, C the fluid concentration and D the diffusion coefficient.

The subjected boundary conditions are [18]:

$$u=u_w(x)=cx, v=0, T=T_w=T_0+bx,\ C=C_w=C_0+dx \text{ at } y=0, \quad (5)$$

$$u\to 0,\ T\to T_\infty=T_0+ax,\ C\to C_\infty=C_0+ex \text{ as } y\to\infty, \quad (6)$$

in which c is the stretching rate, a, b, d, e are dimensional constants and T_0, C_0 are the reference temperature and reference concentration, respectively.

The radiative flux is accounted by employing the Rosseland assumption in the energy equation [12,15]:

$$q_r=-\frac{4\sigma^*}{3k^*}\frac{\partial T^4}{\partial y}, \quad (7)$$

in which σ^* the Stefan-Boltzmann constant and k^* the mean absorption coefficient. Further, the differences of temperature within the flow is assumed to be small such that T^4 may be expressed as a linear function of temperature. Expansion of T^4 about T_∞ via Taylor's series and ignoring higher order terms, we have

$$T^4\cong T_\infty^4+(T-T_\infty)4T_\infty^3=4T_\infty^3T-3T_\infty^4. \quad (8)$$

By employing Eqs. (7) and (8), Eq. (3) has the form

$$\rho C_p\left(u\frac{\partial T}{\partial x}+v\frac{\partial T}{\partial y}\right)=k\frac{\partial^2 T}{\partial y^2}+\frac{16\sigma T_\infty^3}{3k^*}\frac{\partial^2 T}{\partial y^2}. \quad (9)$$

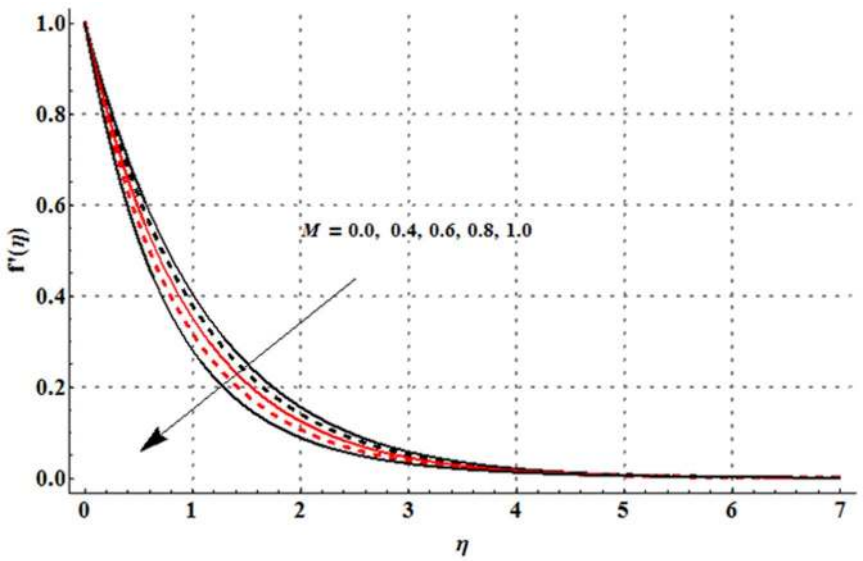

Figure 3. Influence of M on the velocity profile $f'(\eta)$ when $\beta=0.4=Rd$, $\lambda_1=0.5$, $\lambda=0.3=N$, Pr $=1.2$, $S=0.2=S^*$ and $Sc=1.0$.
doi:10.1371/journal.pone.0107858.g003

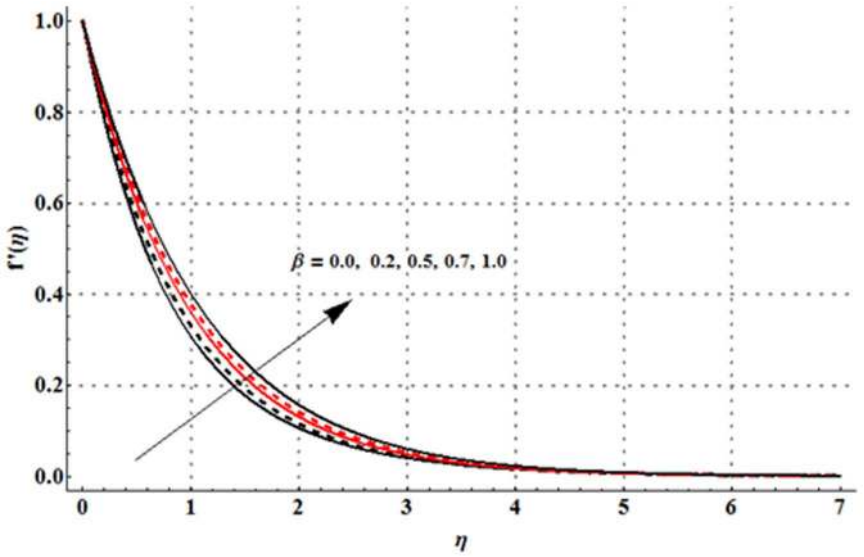

Figure 4. Influence of β on the velocity profile $f'(\eta)$ when $M=0.6$, $Rd=0.4$, $\lambda_1=0.5$, $\lambda=0.3=N$, $\Pr=1.2$, $S=0.2=S^*$ and $Sc=1.0$.
doi:10.1371/journal.pone.0107858.g004

Setting

$$u=cxf'(\eta),\ v=-\sqrt{cv}f(\eta),$$
$$\eta=y\sqrt{\frac{c}{v}},\ \theta(\eta)=\frac{T-T_\infty}{T_w-T_0},\ \phi(\eta)=\frac{C-C_\infty}{C_w-C_0}, \tag{10}$$

equation (1) is satisfied automatically and reduced forms of Eqs. (7)–(10) and (13) are

$$f'''+(1+\lambda_1)(ff''-f'^2)+\beta(f''^2-ff'''')-M(1+\lambda_1)f'+\lambda(1+\lambda_1)(\theta+N\phi)=0, \tag{11}$$

$$(1+\frac{4}{3}Rd)\theta''+\Pr f\theta'-\Pr f'\theta-\Pr Sf'=0, \tag{12}$$

$$\phi''+Scf\phi'-Scf'\phi-ScS^*f'=0, \tag{13}$$

and the boundary conditions in dimensionless form has the following form

$$f=0, f'=1, \theta=1-S, \phi=1-S^* \text{at } \eta=0, \tag{14}$$

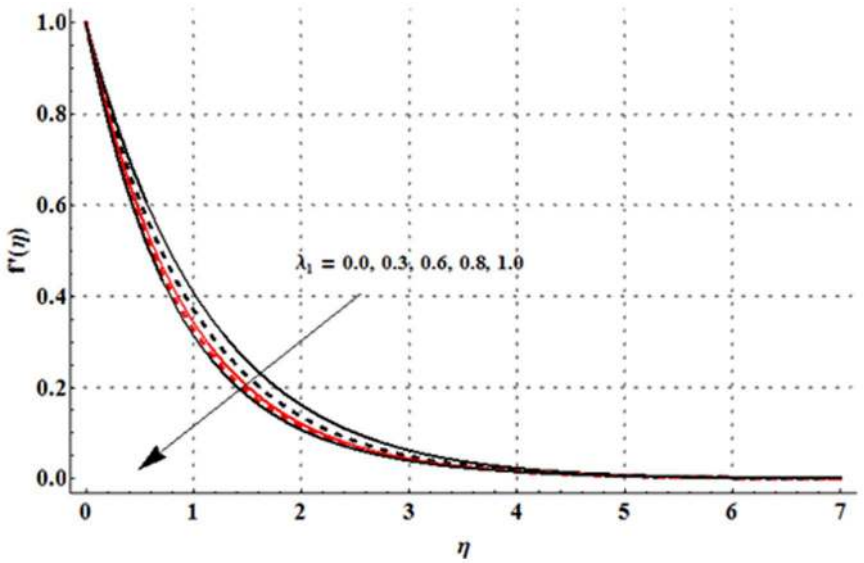

Figure 5. Influence of λ_1 on the velocity profile $f'(\eta)$ when $M=0.6$, $\beta=0.4=Rd$, $\lambda=0.3=N$, $\Pr=1.2$, $S=0.2=S^*$ and $Sc=1.0$.
doi:10.1371/journal.pone.0107858.g005

$$f' \to 0, \theta \to 0, \phi \to 0 \text{ as } \eta \to \infty. \tag{15}$$

Here $\beta = \lambda_2 c$ is the Deborah number, $M = \sigma B_0^2/\rho c$ the magnetic parameter, $\lambda = Gr_x/\mathrm{Re}_x^2$ the thermal buoyancy parameter with $Gr_x = g\beta_T(T - T_\infty)x^3/v^2$ the local Grashof number and $\mathrm{Re}_x = u_w(x)x/v$ the local Reynolds number, $\mathrm{Pr} = v/\alpha$ the Prandtl number, $\alpha = \dfrac{k}{\rho C_p}$ the thermal diffusivity, $Rd = \dfrac{4\sigma^* T_\infty^3}{kk^*}$ the thermal radiation parameter, $S = a/b$ the thermal stratification parameter, $S^* = e/d$ the concentration stratification parameter, $Sc = v/D$ the Schmidt number and f, θ and ϕ the dimensionless velocity, temperature and concentration, respectively.

The skin friction coefficient, the local Nusselt number and the local Sherwood number are

$$C_f = \frac{\tau_w}{\rho_f u_w^2(x)}, Nu_x = \frac{xq_w}{k(T_w - T_\infty)}, Sh_x = \frac{xq_m}{D(C_w - C_\infty)}, \tag{16}$$

where τ_w is the shear stress along the stretching surface, q_w is the surface heat flux and q_m is the surface mass flux. The local skin-friction coefficient, local Nusselt and local Sherwood numbers in dimensionless forms are given below:

$$\begin{aligned} \mathrm{Re}_x^{1/2} C_{fx} &= \frac{1}{1+\lambda_1}(f''(0) + \beta f''(0)), Nu_x/\mathrm{Re}_x^{1/2} \\ &= -(1 + \frac{4}{3}Rd)\theta'(0), Sh_x/\mathrm{Re}_x^{1/2} = -\phi'(0). \end{aligned} \tag{17}$$

Development of the Series Solutions

To develop the homotopic procedure [21–23], we choose the initial guesses and operators in the forms given below:

$$\begin{aligned} &f_0(\eta) = (1 - \exp(-\eta)), \theta_0(\eta) = (1 - S)\exp(-\eta), \\ &\phi_0(\eta) = (1 - S^*)\exp(-\eta), \end{aligned} \tag{18}$$

$$L(f) = f''' - f', L(\theta) = \theta'' - \theta, L(\phi) = \phi'' - \phi, \tag{19}$$

with

$$\begin{aligned} &L(f)(C_1 + C_2 e^{\eta} + C_3 e^{-\eta}) = 0, L(\theta)(C_4 e^{\eta} + C_5 e^{-\eta}) = 0, \\ &L(\phi)(C_5 e^{\eta} + C_7 e^{-\eta}) = 0, \end{aligned} \tag{20}$$

where C_i $(i = 1-7)$ are the arbitrary constants. The zeroth order deformation equations together with the boundary conditions are

$$(1-q)L(f)\left(\hat{f}(\eta; q) - f_0(\eta)\right) = q\hbar_f \mathbf{N}_f\left(\hat{f}(\eta; q), \hat{\theta}(\eta; q), \hat{\phi}(\eta; q)\right), \tag{21}$$

$$(1-q)L(\theta)\left(\hat{\theta}(\eta; q) - \theta_0(\eta)\right) = q\hbar_\theta \mathbf{N}_\theta\left(\hat{f}(\eta; q), \hat{\theta}(\eta, q), \hat{\phi}(\eta; q)\right), \tag{22}$$

$$(1-q)L(\phi)\left(\hat{\phi}(\eta; q) - \phi_0(\eta)\right) = q\hbar_\phi \mathbf{N}_\phi\left(\hat{f}(\eta; q), \hat{\theta}(\eta, q), \hat{\phi}(\eta; q)\right), \tag{23}$$

$$\begin{aligned} &\hat{f}(0; q) = 0, \hat{f}'(0; q) = 1, \hat{f}'(\infty; q) = 0, \\ &\hat{\theta}(0, q) = 1 - S, \hat{\theta}(\infty, q) = 0, \hat{\phi}(0; q) = 1 - S^*, \hat{\phi}(\infty; q) = 0, \end{aligned} \tag{24}$$

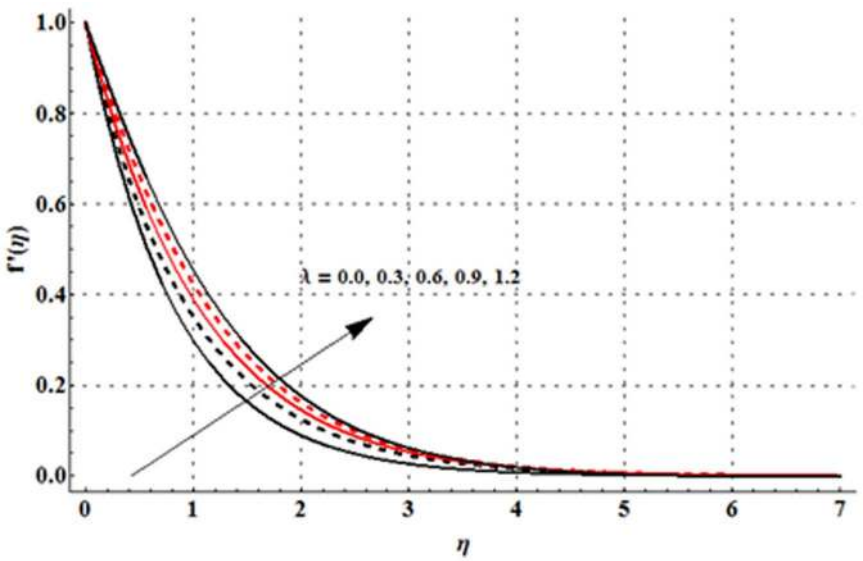

Figure 6. Influence of λ on the velocity profile $f'(\eta)$ when $M = 0.6$, $\beta = 0.4 = Rd$, $\lambda_1 = 0.5$, $N = 0.3$, $\mathrm{Pr} = 1.2$, $S = 0.2 = S^*$ and $Sc = 1.0$.
doi:10.1371/journal.pone.0107858.g006

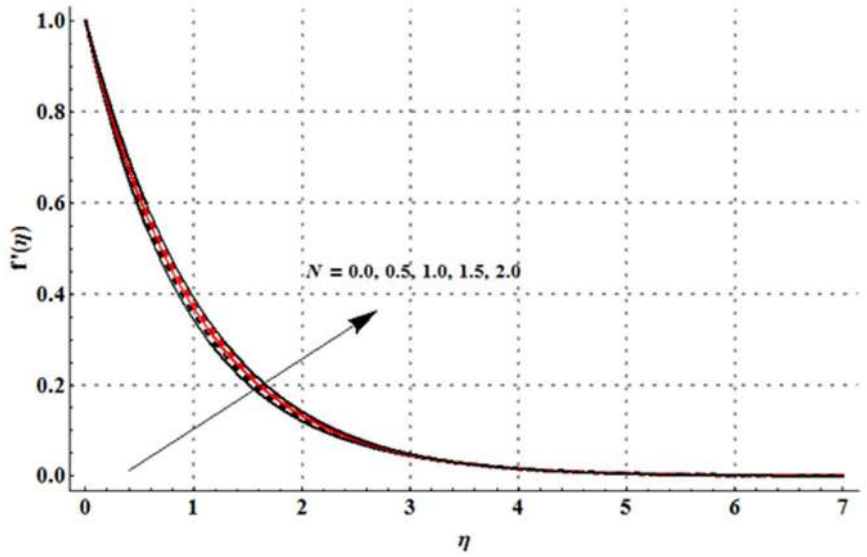

Figure 7. Influence of N on the velocity profile $f'(\eta)$ when $M=0.6$, $\beta=0.4=Rd$, $\lambda_1=0.5$, $\lambda=0.3$, $\Pr=1.2$, $S=0.2=S^*$ and $Sc=1.0$.
doi:10.1371/journal.pone.0107858.g007

$$\begin{aligned}&\mathbf{N}_f[\hat{f}(\eta,q),\hat{\theta}(\eta,q),\hat{\phi}(\eta,q)]=\\&\frac{\partial^3\hat{f}(\eta,q)}{\partial\eta^3}+(1+\lambda_1)\left(\hat{f}(\eta,q)\frac{\partial^2\hat{f}(\eta,q)}{\partial\eta^2}-\left(\frac{\partial\hat{f}(\eta,q)}{\partial\eta}\right)^2\right)\\&+\beta\left(\left(\frac{\partial^2\hat{f}\eta,q)}{\partial\eta^2}\right)^2-\hat{f}(\eta,q)\frac{\partial^4\hat{f}(\eta,q)}{\partial\eta^4}\right)-(1+\lambda_1)M\frac{\partial\hat{f}(\eta,q)}{\partial\eta},\\&+\lambda(1+\lambda_1)(\hat{\theta}\eta,q)+N\hat{\phi}(\eta,q)),\end{aligned}\tag{25}$$

$$\begin{aligned}\mathbf{N}_\theta[\hat{\theta}(\eta,q),\hat{f}(\eta,q),\hat{\phi}(\eta,q)]&=(1+\frac{4}{3}Rd)\frac{\partial^2\hat{\theta}(\eta,p)}{\partial\eta^2}-\Pr\hat{\theta}(\eta,p)\frac{\partial\hat{f}(\eta,p)}{\partial\eta}\\&+\Pr\hat{f}(\eta,p)\frac{\partial\hat{\theta}(\eta,p)}{\partial\eta}-\Pr S\frac{\partial\hat{f}(\eta,p)}{\partial\eta},\end{aligned}\tag{26}$$

$$\begin{aligned}\mathbf{N}_\phi[\hat{\phi}(\eta,q),\hat{\theta}(\eta,q),\hat{f}(\eta,q)]&=\frac{\partial^2\hat{\phi}(\eta,q)}{\partial\eta^2}-Sc\hat{\phi}(\eta,q)\frac{\partial\hat{f}(\eta,p)}{\partial\eta}\\&+Sc\hat{f}(\eta,p)\frac{\partial\hat{\phi}(\eta,q)}{\partial\eta}-ScS^*\frac{\partial\hat{f}(\eta,p)}{\partial\eta},\end{aligned}\tag{27}$$

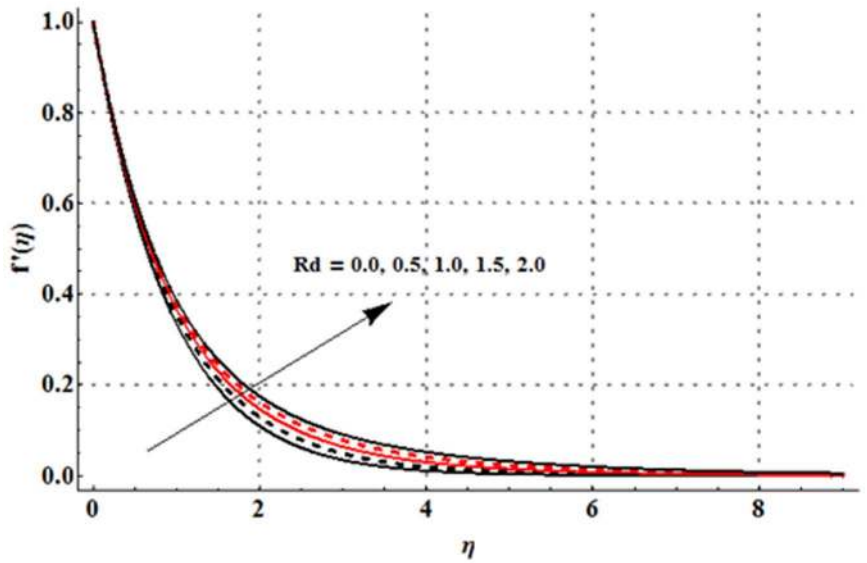

Figure 8. Influence of Rd on the velocity profile $f'(\eta)$ when $M=0.6$, $\beta=0.4$, $\lambda_1=0.5$, $\lambda=0.3=N$, $\Pr=1.2$, $S=0.2=S^*$ and $Sc=1.0$.
doi:10.1371/journal.pone.0107858.g008

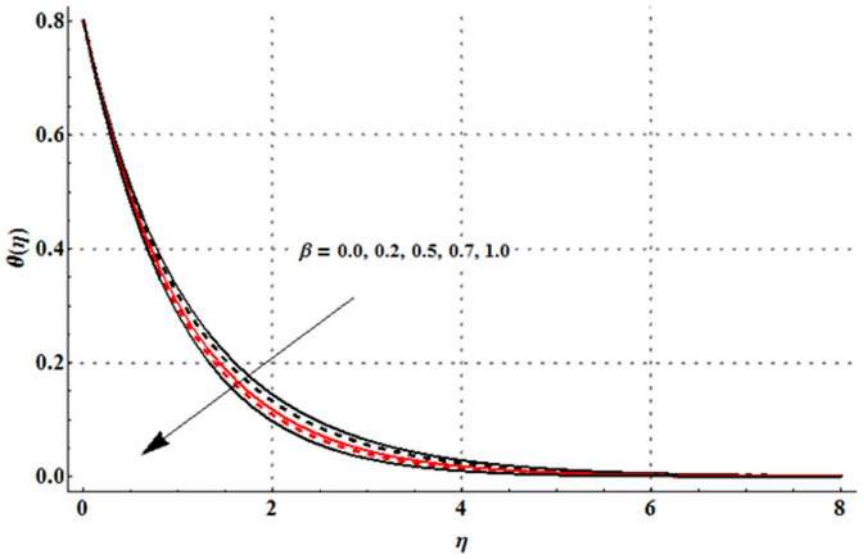

Figure 9. Influence of M on the temperature profile $\theta(\eta)$ when $\beta=0.4=Rd$, $\lambda_1=0.5$, $\lambda=0.3=N$, $\Pr=1.2$, $S=0.2=S^*$ and $Sc=1.0$.
doi:10.1371/journal.pone.0107858.g009

where q is an embedding parameter, $\hbar_f$, $\hbar_\theta$ and $\hbar_\phi$ the non-zero auxiliary parameters and $\mathbf{N}_f$, $\mathbf{N}_\theta$ and $\mathbf{N}_\phi$ the nonlinear operators. For $q=0$ and $q=1$ one has

$$\begin{aligned}&\hat{f}(\eta;\,0)=f_0(\eta),\hat{\theta}(\eta,0)=\theta_0(\eta),\hat{\phi}(\eta,0)=\phi_0(\eta),\\&\hat{f}(\eta;\,1)=f(\eta),\hat{\theta}(\eta,1)=\theta(\eta),\hat{\phi}(\eta,1)=\phi(\eta).\end{aligned}\tag{28}$$

When variation of q is taken into account from 0 to 1 then $f(\eta,q)$, $\theta(\eta,q)$ and $\phi(\eta,q)$ vary from $f_0(\eta)$, $\theta_0(\eta)$, $\phi_0(\eta)$ to $f(\eta)$, $\theta(\eta)$ and $\phi(\eta)$. We expand f, θ and ϕ in the following forms [24–26]:

$$f(\eta,q)=f_0(\eta)+\sum_{m=1}^{\infty}f_m(\eta)q^m,f_m(\eta)=\frac{1}{m!}\frac{\partial^m f(\eta;\,q)}{\partial\eta^m}\Big|_{q=0},\tag{29}$$

$$\theta(\eta,p)=\theta_0(\eta)+\sum_{m=1}^{\infty}\theta_m(\eta)q^m,\theta_m(\eta)=\frac{1}{m!}\frac{\partial^m\theta(\eta;\,q)}{\partial\eta^m}\Big|_{q=0},\tag{30}$$

$$\phi(\eta,p)=\phi_0(\eta)+\sum_{m=1}^{\infty}\phi_m(\eta)q^m,\phi_m(\eta)=\frac{1}{m!}\frac{\partial^m\phi(\eta;\,q)}{\partial\eta^m}\Big|_{q=0},\tag{31}$$

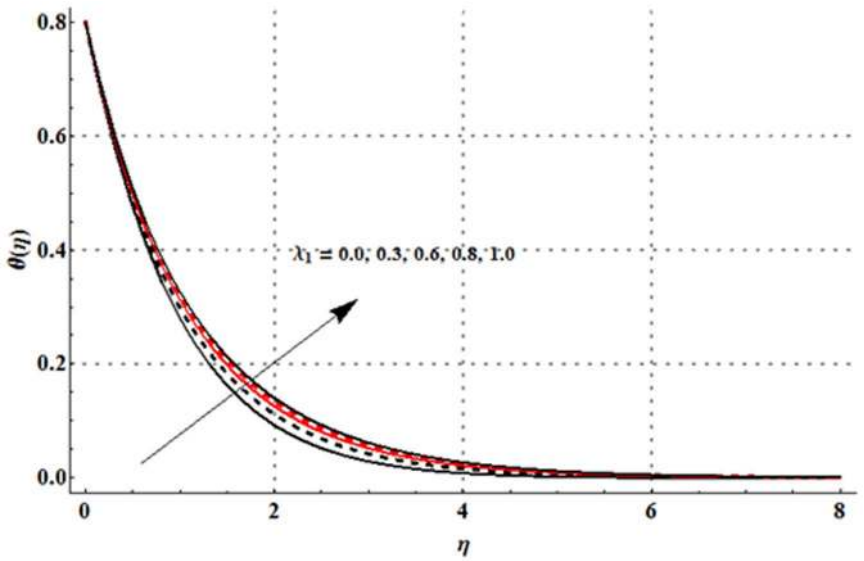

Figure 10. Influence of β on the temperature profile $\theta(\eta)$ when $M=0.6$, $Rd=0.4$, $\lambda_1=0.5$, $\lambda=0.3=N$, $\Pr=1.2$, $S=0.2=S^*$ and $Sc=1.0$.
doi:10.1371/journal.pone.0107858.g010

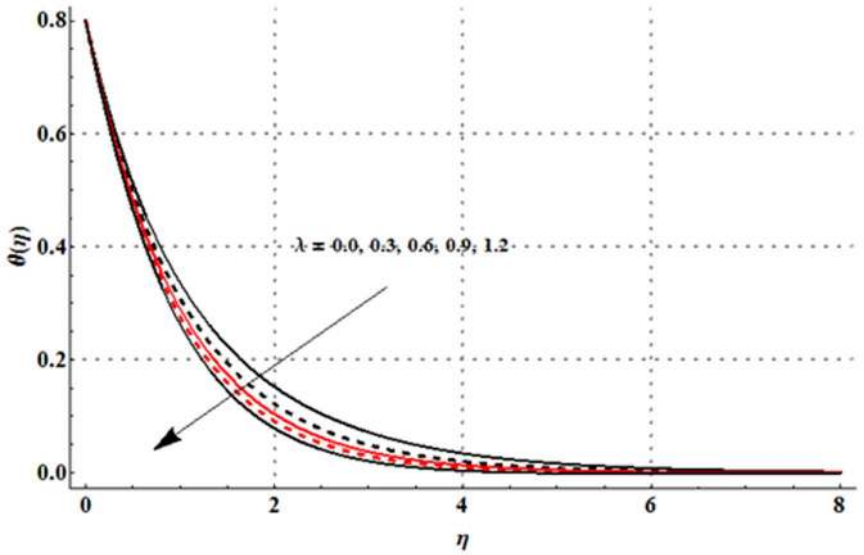

Figure 11. Influence of λ_1 on the temperature profile $\theta(\eta)$ when $M=0.6$, $\beta=0.4=Rd$, $\lambda=0.3=N$, $\Pr=1.2$, $S=0.2=S^*$ and $Sc=1.0$.
doi:10.1371/journal.pone.0107858.g011

where the convergence of above series strongly depends upon $\hbar_f$, $\hbar_\theta$ and $\hbar_\phi$. Considering that $\hbar_f$, $\hbar_\theta$ and $\hbar_\phi$ are selected properly such that Eqs. (29)–(31) converge for $q=1$ and thus [27,28]:

$$f(\eta)=f_0(\eta)+\sum_{m=1}^{\infty} f_m(\eta), \tag{32}$$

$$\theta(\eta)=\theta_0(\eta)+\sum_{m=1}^{\infty} \theta_m(\eta), \tag{33}$$

$$\phi(\eta)=\phi_0(\eta)+\sum_{m=1}^{\infty} \phi_m(\eta). \tag{34}$$

The general solutions are derived as follows:

$$f_m(\eta)=f_m^*(\eta)+C_1+C_2e^{\eta}+C_3e^{-\eta}, \tag{35}$$

$$\theta_m(\eta)=\theta_m^*(\eta)+C_4e^{\eta}+C_5e^{-\eta}, \tag{36}$$

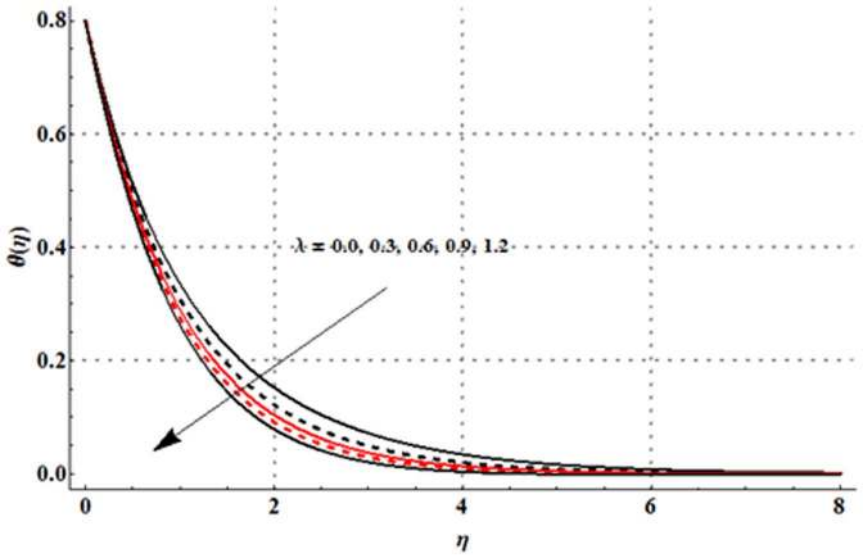

Figure 12. Influence of λ on the temperature profile $\theta(\eta)$ when $M=0.6$, $\beta=0.4=Rd$, $\lambda_1=0.5$, $N=0.3$, $\Pr=1.2$, $S=0.2=S^*$ and $Sc=1.0$.
doi:10.1371/journal.pone.0107858.g012

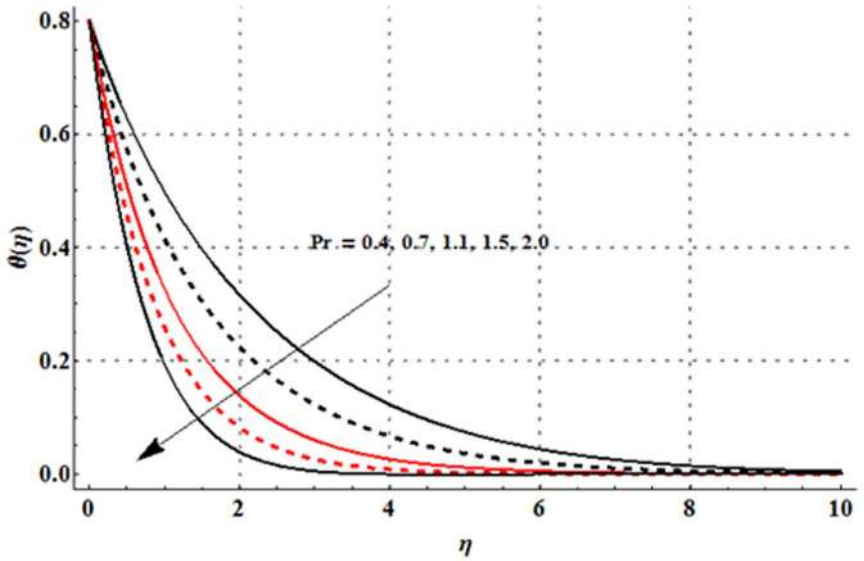

Figure 13. Influence of Pr **on the temperature profile** $\theta(\eta)$ **when** $M=0.6$, $\beta=0.4=Rd$, $\lambda_1=0.5$, $\lambda=0.3=N$, $S=0.2=S^*$ **and** $Sc=1.0$.
doi:10.1371/journal.pone.0107858.g013

$$\phi_m(\eta)=\phi_m^*(\eta)+C_6e^{\eta}+C_7e^{-\eta}, \tag{37}$$

where $f_m^*(\eta)$, $\theta_m^*(\eta)$, and $\phi_m^*(\eta)$ are the special solutions.

Analysis and Discussion

The coupled nonlinear ordinary differential equations are solved via homotopy analysis method. The convergence of derived homotopic solutions depend on the suitable values of auxiliary parameters $\hbar_f$, $\hbar_\theta$ and $\hbar_\phi$. Hence the $\hbar-$ curves of functions $f(\eta)$, $\theta(\eta)$ and $\phi(\eta)$ are drawn at 21^{ist} -order of approximations to choose the admissible values of $\hbar_f$, $\hbar_\theta$ and $\hbar_\phi$. From Fig. 2 we have seen that the range of admissible values of $\hbar_f$, $\hbar_\theta$ and $\hbar_\phi$ are $-1.15\le\hbar_f\le-0.1$, $-1.20\le\hbar_\theta\le-0.10$ and $-1.20\le\hbar_\phi\le-0.30$. Table 1 also shows that the developed homotopic solutions are convergent in the whole region of η when $\hbar_f=-0.6=\hbar_\theta=\hbar_\phi$.

The dimensionless velocity profile $f'(\eta)$ for different values of magnetic parameter M, Deborah number β, ratio of relaxation to retardation times λ_1, thermal buoyancy parameter λ, concentration buoyancy parameter N and radiation parameter Rd is sketched in the Figs. 3–8. It is noticed from Fig. 3 that the velocity profile and momentum boundary layer thickness is reduced when larger values of magnetic parameter are used. Here the magnetic parameter involves the Lorentz force. Lorentz force has an ability to resist the fluid flow. Such resistance in fluid flow leads to a reduction in the velocity profile. From Fig. 4 it is observed that larger Deborah number shows higher velocity and thicker momentum boundary layer thickness. From the definition of

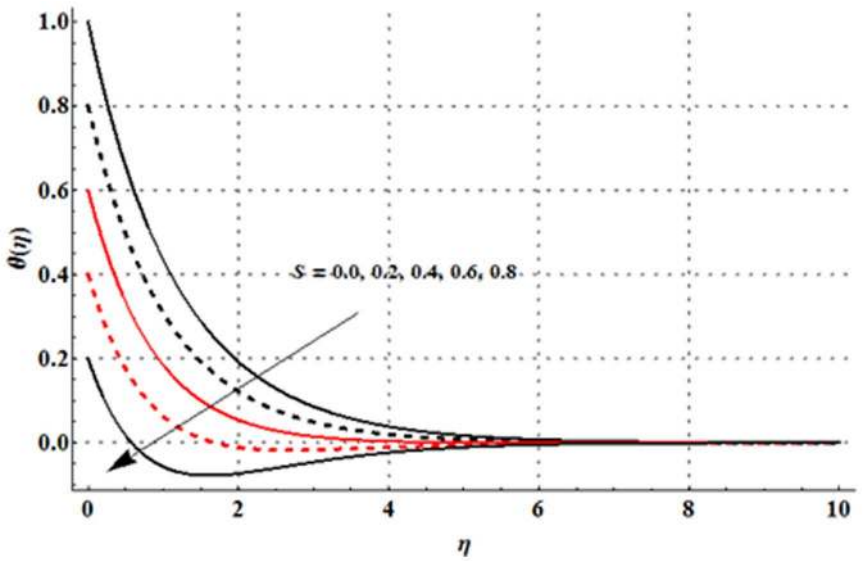

Figure 14. Influence of S **on the temperature profile** $\theta(\eta)$ **when** $M=0.6$, $\beta=0.4=Rd$, $\lambda_1=0.5$, $\lambda=0.3=N$, $\Pr=1.2$, $S^*=0.2$ **and** $Sc=1.0$.
doi:10.1371/journal.pone.0107858.g014

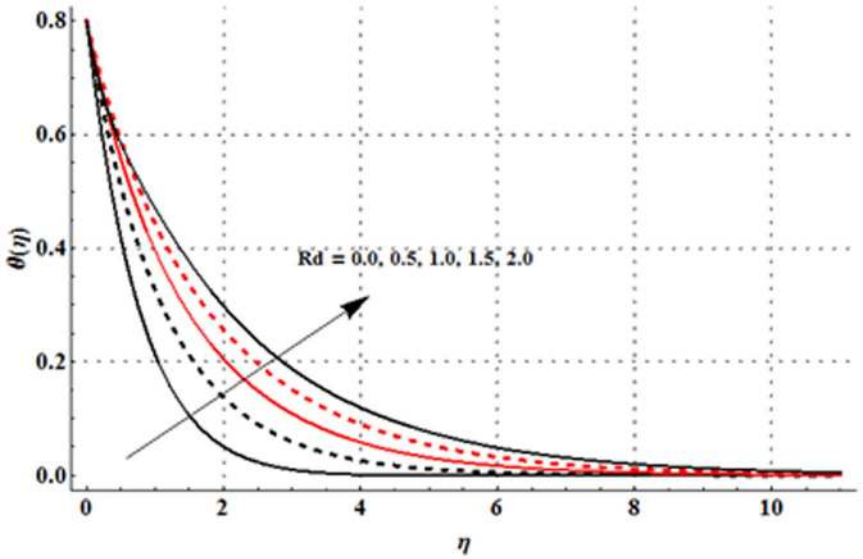

Figure 15. Influence of Rd on the temperature profile $\theta(\eta)$ when $M=0.6$, $\beta=0.4$, $\lambda_1=0.5$, $\lambda=0.3=N$, $\Pr=1.2$, $S=0.2=S^*$ and $Sc=1.0$.
doi:10.1371/journal.pone.0107858.g015

Deborah number, one can see that the Deborah number is directly proportional to the retardation time. Larger Deborah number has higher retardation time. Such higher retardation time gives rise to the fluid flow due to which the velocity profile is enhanced. Fig. 5 illustrates the impact of ratio of relaxation to retardation times on the velocity field. This Fig. shows that the velocity and its related boundary layer thickness are decreasing functions of ratio of relaxation to retardation times. Fig. 6 depicts that an increase in thermal buoyancy parameter leads to an increase in the velocity profile. Thermal buoyancy parameter depends on the buoyancy force. Larger buoyancy parameter has stronger buoyancy force. Such stronger buoyancy force acts as an agent and causes to an increase in the fluid velocity. Fig. 7 elucidates that both velocity profile and its related momentum boundary layer thickness are enhanced with an increase in the concentration buoyancy parameter. The change in velocity distribution function for various values of radiation parameter is examined in Fig. 8. Here we observed that the velocity distribution function is increased when we increase the values of radiation parameter.

The variations in the non-dimensional temperature distribution function $\theta(\eta)$ correspond to different values of magnetic parameter M, Deborah number β, ratio of relaxation to retardation times λ_1, thermal buoyancy parameter λ, Prandtl number $\Pr$, thermal stratification parameter S and radiation parameter Rd are examined in the Figs. 9–15. From Fig. 9 it is seen that the temperature profile and thermal boundary layer thickness are enhanced for the larger magnetic parameter. Here stronger Lorentz force corresponds to the larger magnetic parameter. This stronger Lorentz force has an ability to increase the temperature. Figs. 10 and 11 depict that the Deborah number and ratio of

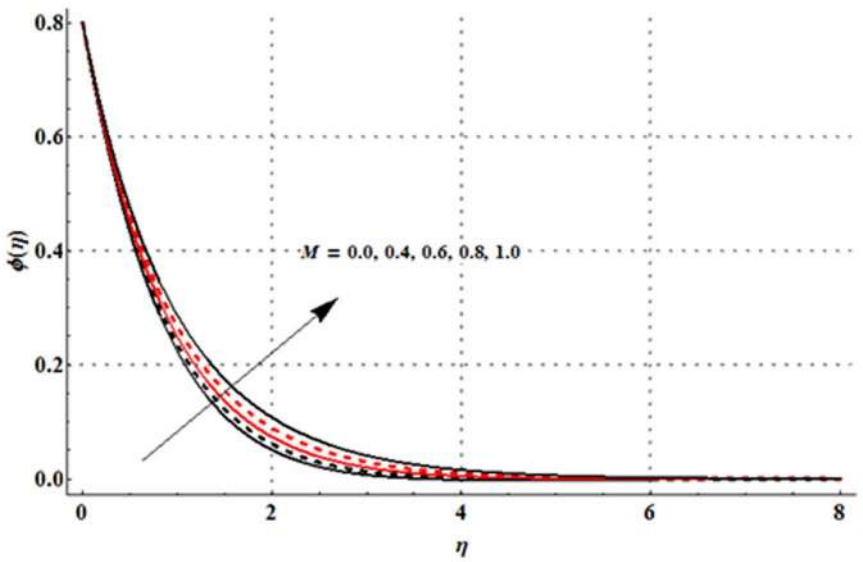

Figure 16. Influence of M on the concentration profile $\phi(\eta)$ when $\beta=0.4=Rd$, $\lambda_1=0.5$, $\lambda=0.3=N$, $\Pr=1.2$, $S=0.2=S^*$ and $Sc=1.0$.
doi:10.1371/journal.pone.0107858.g016

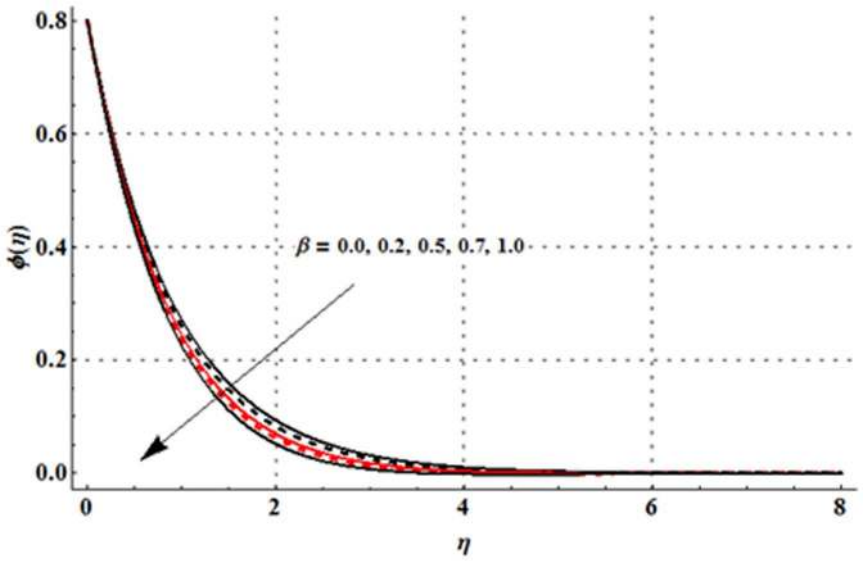

Figure 17. Influence of β on the concentration profile $\phi(\eta)$ when $M=0.6$, $Rd=0.4$, $\lambda_1=0.5$, $\lambda=0.3=N$, $\Pr=1.2$, $S=0.2=S^*$ and $Sc=1.0$.
doi:10.1371/journal.pone.0107858.g017

relaxation to retardation times have quite reverse effects on the temperature field and thermal boundary layer thickness. Temperature is decreased with an increase in the Deborah number but an enhancement in the temperature is observed for larger ratio of relaxation to retardation times. Fig. 12 illustrates that an increase in the thermal buoyancy parameter leads to a reduction in the temperature profile and thermal boundary layer thickness. From Fig. 13 we observed that lower temperature and thinner thermal boundary layer thickness correspond to an increase in the Prandtl number. Prandtl number is the ratio of momentum to thermal diffusivities. An enhancement in the Prandtl number implies to higher momentum diffusivity and lower thermal diffusivity. Such variation in momentum and thermal diffusivities shows a reduction in the temperature profile and thermal boundary layer thickness. Fig. 14 is sketched for temperature field when different values of thermal stratification parameter are taken into account. We have seen that the temperature profile is reduced when we increase the values of thermal stratification parameter. It is also noticed that the case of prescribed surface temperature is obtained when $S=0$. Physically, the difference between the surface temperature and ambient temperature is decreased when larger values of thermal stratification parameter are used. This change in surface and ambient temperatures leads to a decrease in the temperature profile. From Fig. 15 we noticed that higher temperature and thicker thermal boundary layer thickness correspond to the larger radiation parameter. Here larger radiation parameter gives more heat to fluid due to which the temperature profile is enhanced.

The effects of magnetic parameter M, Deborah number β, ratio of relaxation to retardation times λ_1, concentration stratification

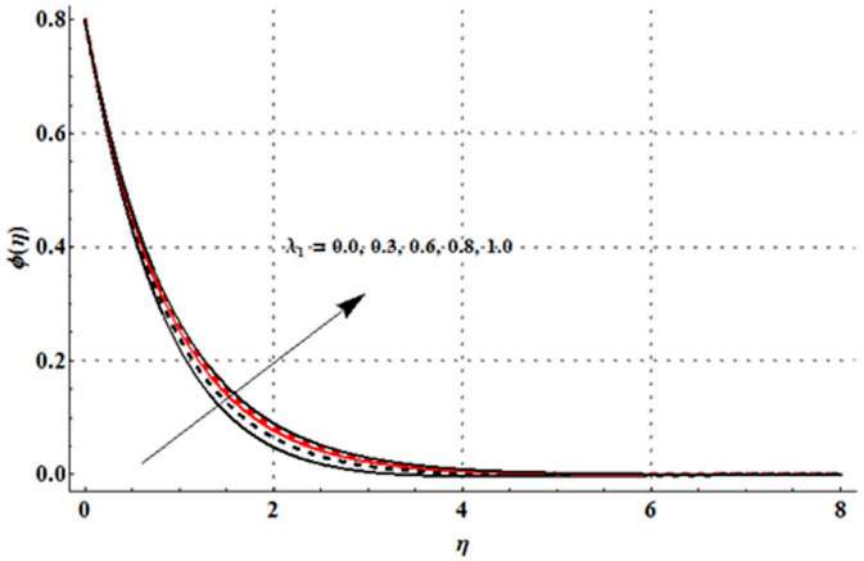

Figure 18. Influence of λ_1 on the concentration profile $\phi(\eta)$ when $M=0.6$, $\beta=0.4=Rd$, $\lambda=0.3=N$, $\Pr=1.2$, $S=0.2=S^*$ and $Sc=1.0$.
doi:10.1371/journal.pone.0107858.g018

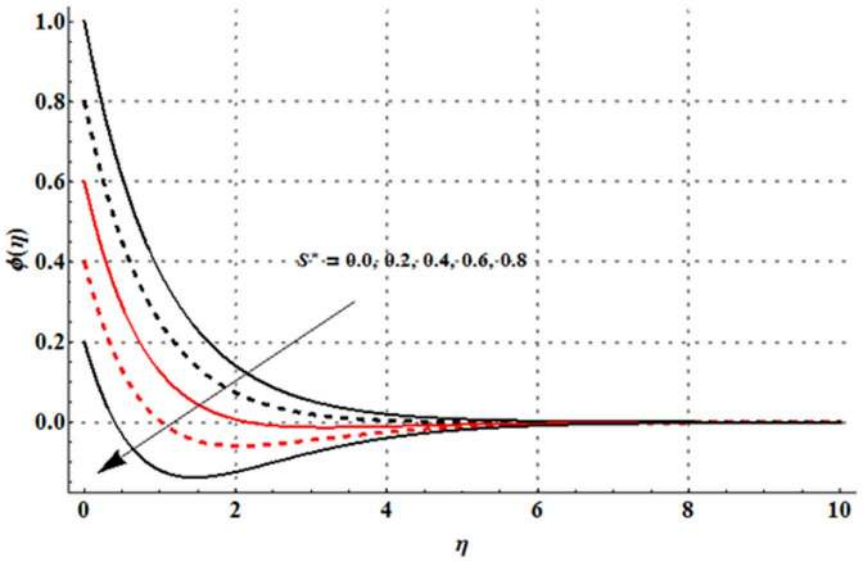

Figure 19. Influence of S^* on the concentration profile $\phi(\eta)$ when $M=0.6$, $\beta=0.4=Rd$, $\lambda_1=0.5$, $\lambda=0.3=N$, $\Pr=1.2$, $S=0.2$ and $Sc=1.0$.
doi:10.1371/journal.pone.0107858.g019

parameter S^* and Schmidt number Sc on the concentration field $\phi(\eta)$ are shown in the Figs. 16–20. Fig. 16 elucidates that concentration profile and its associated boundary layer thickness are increased with an increase in the magnetic parameter. From Figs. 17 and 18, we observed that the concentration is decreased for larger Deborah number but the larger values of ratio of relaxation to retardation times give rise to the concentration field. Impact of concentration stratification parameter on the concentration profile is examined in Fig. 19. From this Fig. it is observed that the concentration profile is reduced with an increase in the concentration stratification parameter. Further prescribed surface concentration case is achieved when we use $S^*=0$. An increase in Schmidt number leads to a reduction in the concentration profile and its related boundary layer thickness (see Fig. 20).

The numerical values of $f''(0)$, $\theta'(0)$ and $\phi'(0)$ at different order of HAM approximations are analyzed in Table 1 when $M=0.6$, $\beta=0.6=Rd$, $\lambda_1=0.5$, $\lambda=0.3=N$, $\Pr=1.2$, $S=0.2=S^*$, $Sc=1.0$ and $\hbar_f=-0.7=\hbar_\theta=\hbar_\phi$. From this Table it is noticed that the values of $f''(0)$ and $\theta'(0)$ start to repeat from 24th-order of deformations. On the other hand the values of $\phi'(0)$ converge from 28th-order of approximations. Table 2 presents the numerical values of skin-friction coefficient for different values of M, β, λ_1, λ and N when $\Pr=1.2$, $S=0.2=S^*$, $Rd=0.4$, and $Sc=1.0$. It is observed that the values of skin-friction coefficient are larger when we increase the values of M and β but these values are smaller for larger λ_1, λ and N. Table 3 is computed to examine the values of skin-friction coefficient for different values of $\Pr$, S, S^*, Rd and Sc when $M=0.6$, $\beta=0.4$, $\lambda_1=0.5$ and $\lambda=0.3=N$. This Table shows that the values of skin-friction coefficient are

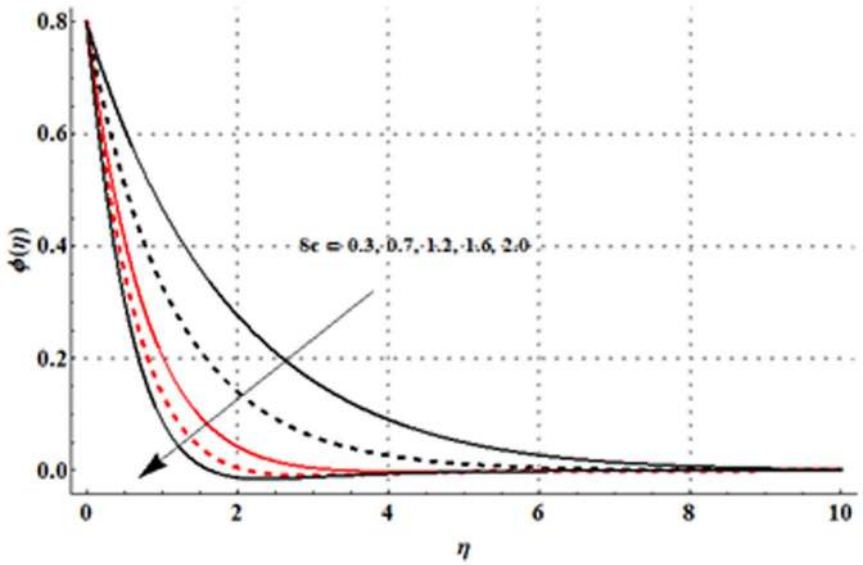

Figure 20. Influence of Sc on the concentration profile $\phi(\eta)$ when $M=0.6$, $\beta=0.4=Rd$, $\lambda_1=0.5$, $\lambda=0.3=N$, $\Pr=1.2$ and $S=0.2=S^*$.
doi:10.1371/journal.pone.0107858.g020

Table 2. Values of skin-friction coefficient $\frac{1}{1+\lambda_1}(f''(0)+\beta f''(0))$ for different values of M, β, λ_1, λ and N when $\Pr=1.2$, $S=0.2=S^*$, $Rd=0.4$ and $Sc=1.0$.

M	β	λ_1	λ	N	$\frac{1}{1+\lambda_1}(f''(0)+\beta f''(0))$
0.0	0.4	0.5	0.3	0.3	0.82197
0.4					0.89699
0.8					1.09849
0.6	0.0	0.5	0.3	0.3	0.81634
	0.3				0.94515
	0.7				1.09609
0.6	0.4	0.0	0.3	0.3	1.23185
		0.6			0.95028
		1.0			0.84010
0.6	0.4	0.5	0.0	0.3	1.12665
			0.4		0.81119
			0.7		0.94018
0.6	0.4	0.5	0.3	0.0	1.01394
				0.4	0.97514
				0.7	0.94646

doi:10.1371/journal.pone.0107858.t002

increased with an increase in $\Pr$, S, S^* and Sc but a decrease is noticed for the larger Rd. Numerical values of local Nusselt and Sherwood numbers for various values of M, β, λ_1, λ, N, $\Pr$, S, S^*, Rd and Sc are observed in the Tables 4 and 5. From these Tables we have seen that the values of local Nusselt number are larger in comparison to the values of local Sherwood number when we used the values of M, β, λ_1, λ, N, S and S^*.

Conclusions

We examined the effects of thermal and concentration stratifications in mixed convective radiative flow of Jeffrey fluid in this attempt. The main observations that we found in this investigation are as follows:

- We have to compute 28th-order of HAM deformations for the convergent solutions.

Table 3. Values of skin-friction coefficient $\frac{1}{1+\lambda_1}(f''(0)+\beta f''(0))$ for different values of $\Pr$, S, S^*, Rd and Sc when $M=0.6$, $\beta=0.4$, $\lambda_1=0.5$ and $\lambda=0.3=N$.

$\Pr$	S	S^*	Rd	Sc	$\frac{1}{1+\lambda_1}(f''(0)+\beta f''(0))$
0.7	0.2	0.2	0.4	1.0	0.96396
1.0					0.97756
1.3					0.98797
1.2	0.0	0.2	0.4	1.0	0.94859
	0.5				1.03868
	0.7				1.07436
1.2	0.2	0.0	0.4	1.0	0.97432
		0.5			1.00044
		0.7			1.01086
1.2	0.2	0.2	0.0	1.0	1.00186
			0.5		0.98145
			0.8		0.96839
1.2	0.2	0.2	0.4	0.8	0.98212
				2.0	0.99263
				2.5	0.99495

doi:10.1371/journal.pone.0107858.t003

Table 4. Values of local Nusselt number $-\left(1+\frac{4}{3}Rd\right)\theta'(0)$ and local Sherwood number $-\phi'(0)$ for different values of M, β, λ_1, λ and N when $\Pr=1.2$, $S=0.2=S^*$, $Rd=0.4$ and $Sc=1.0$.

M	β	λ_1	λ	N	$-\left(1+\frac{4}{3}Rd\right)\theta'(0)$	$-\phi'(0)$
0.0	0.4	0.5	0.3	0.3	1.24653	0.95218
0.4					1.22027	0.93431
0.8					1.15112	0.88693
0.6	0.0	0.5	0.3	0.3	1.14034	0.87924
	0.3				1.17885	0.90598
	0.7				1.21882	0.93328
0.6	0.4	0.0	0.3	0.3	1.25054	0.95473
		0.6			1.18031	0.90697
		1.0			1.14782	0.88445
0.6	0.4	0.5	0.0	0.3	1.12659	0.87086
			0.4		1.20514	0.92399
			0.7		1.24331	0.95029
0.6	0.4	0.5	0.3	0.0	1.18090	0.90734
				0.4	1.19273	0.91552
				0.7	1.20103	0.92126

doi:10.1371/journal.pone.0107858.t004

- Deborah number β and ratio of relaxation to retardation times have reverse effects on the velocity profile $f'(\eta)$.
- The effects of thermal buoyancy parameters on the velocity field $f'(\eta)$ are more pronounced in comparison to concentration buoyancy parameter.
- An increase in thermal stratification parameter S leads to a reduction in the temperature field and thermal boundary layer thickness.
- The temperature profile and thermal boundary layer thickness are enhanced when radiation parameter Rd is increased.
- The concentration field and its associated boundary layer thickness are decreasing functions of concentration stratification parameter S^*.
- Numerical values of skin-friction coefficient are increased by increasing S and S^*.

Table 5. Values of local Nusselt number $-\left(1+\frac{4}{3}Rd\right)\theta'(0)$ and local Sherwood number $-\phi'(0)$ for different values of $\Pr$, S, S^*, Rd and Sc when $M=0.6$, $\beta=0.4$, $\lambda_1=0.5$ and $\lambda=0.3=N$.

$\Pr$	S	S^*	Rd	Sc	$-\left(1+\frac{4}{3}Rd\right)\theta'(0)$	$-\phi'(0)$
0.7	0.2	0.2	0.4	1.0	0.84401	0.93252
1.0					1.05959	0.91966
1.3					1.25180	0.91100
1.2	0.0	0.2	0.4	1.0	1.31047	0.92744
	0.5				1.00330	0.89150
	0.7				0.87521	0.87585
1.2	0.2	0.0	0.4	1.0	1.19544	0.99065
		0.5			1.18137	0.79709
		0.7			1.17562	0.71897
1.2	0.2	0.2	0.0	1.0	1.01578	0.90118
			0.5		1.22660	0.91628
			0.8		1.32621	0.92373
1.2	0.2	0.2	0.4	0.8	1.19275	0.78950
				2.0	1.18395	1.40976
				2.5	1.18275	1.61211

doi:10.1371/journal.pone.0107858.t005

- The larger values of S and S^* correspond to the lower values of local Nusselt and local Sherwood numbers.

Author Contributions

Conceived and designed the experiments: T. Hayat T. Hussain SAS AA. Performed the experiments: T. Hayat T. Hussain SAS AA. Analyzed the data: T. Hayat T. Hussain SAS AA. Contributed reagents/materials/analysis tools: T. Hayat T. Hussain SAS AA. Wrote the paper: T. Hayat T. Hussain SAS AA.

References

1. Kothandapani M, Srinivas S (2008) Peristaltic transport of a Jeffrey fluid under the effect of magnetic field in an asymmetric channel. Int J Non-Linear Mech 43: 915–924.
2. Tripathi D, Ali N, Hayat T, Chaube MK, Hendi AA (2011) Peristaltic flow of MHD Jeffrey fluid through a finite length cylindrical tube. Appl Math Mech-Engl Edit 32: 1148–1160.
3. Hayat T, Shehzad SA, Qasim M, Obaidat S (2012) Radiative flow of Jeffery fluid in a porous medium with power law heat flux and heat source. Nuclear Eng Design 243: 15–19.
4. Turkyilmazoglu M, Pop I (2013) Exact analytical solutions for the flow and heat transfer near the stagnation point on a stretching/shrinking sheet in a Jeffrey fluid. Int J Heat Mass Transfer 57: 82–88.
5. Shehzad SA, Alsaadi FE, Monaquel SJ, Hayat T (2013) Soret and Dufour effects on the stagnation point flow of Jeffery fluid with convective boundary conditions. Europ Phys J Plus 128: 56.
6. Ramzan M, Farooq M, Alsaedi A, Hayat T (2013) MHD three-dimensional flow of couple stress fluid with Newtonian heating. Europ Phys J Plus 128: 49.
7. Sheikholeslami M, Gorji-Bandpy M, Ganji DD (2013) Numerical investigation of MHD effects on Al_2O_3-water nanofluid flow and heat transfer in a semi-annulus enclosure using LBM. Energy 60: 501–510.
8. Rashidi MM, Abelman S, Mehr NF (2013) Entropy generation in steady MHD flow due to a rotating porous disk in a nanofluid. Int J Heat Mass Transfer 62: 515–525.
9. Makinde OD, Khan WA, Khan ZH (2013) Buoyancy effects on MHD stagnation point flow and heat transfer of a nanofluid past a convectively heated stretching/shrinking sheet. Int J Heat Mass Transfer 62: 526–533.
10. Turkyilmazoglu M (2013) The analytical solution of mixed convection heat transfer and fluid flow of a MHD viscoelastic fluid over a permeable stretching surface. Int J Mech Sci 77: 263–268.
11. Shehzad SA, Alsaedi A, Hayat T (2013) Hydromagnetic steady flow of Maxwell fluid over a bidirectional stretching surface with prescribed surface temperature and prescribed surface heat flux. Plos One 8: e68139.
12. Turkyilmazoglu M, Pop I (2013) Heat and mass transfer of unsteady natural convection flow of some nanofluids past a vertical infinite flat plate with radiation effect. Int J Heat Mass Transfer 59: 167–171.
13. Hayat T, Waqas M, Shehzad SA, Alsaedi A (2013) Mixed convection radiative flow of Maxwell fluid near a stagnation point with convective condition. J Mech 29: 403–409.
14. Shehzad SA, Alsaedi A, Hayat T (2013) Influence of thermophoresis and Joule heating on the radiative flow of Jeffrey fluid with mixed convection. Braz J Chem Eng 30: 897–908.
15. Moradi A, Ahmadikia H, Hayat T, Alsaedi A (2013) On mixed convection radiation interaction about an inclined plate through a porous medium. Int J Thermal Sci 64: 129–136.
16. Hayat T, Shehzad SA, Al-Sulami HH, Asghar S (2013) Influence of thermal stratification on the radiative flow of Maxwell fluid. J Braz Soc Mech Sci Eng 35: 381–389.
17. Shehzad SA, Qasim M, Alsaedi A, Hayat T, Alhuthali MS (2013) Combined effects of thermal stratification and thermal radiation in mixed convection flow of thixotropic fluid. Europ Phys J Plus 128: 7.
18. Ibrahim W, Makinde OD (2013) The effect of double stratification on boundary-layer flow and heat transfer of nanofluid over a vertical plate. Comput Fluids 86: 433–441.
19. Srinivasacharya D, Upendar M (2013) Effect of double stratification on MHD free convection in a micropolar fluid. J Egypt Math Soc 21: 370–378.
20. Srinivasacharya D, Surender (2014) Non-Darcy mixed convection in a doubly stratified porous medium with Soret-Dufour effects. Int J Eng Math 2014: 126218.
21. Liao SJ (2009) Notes on the homotopy analysis method: Some definitions and theorems. Commun Nonlinear Sci Numer Simulat 14: 983–997.
22. Turkyilmazoglu M (2010) A note on the homotopy analysis method. Appl Math Lett 23: 1226–1230.
23. Turkyilmazoglu M (2012) Solution of the Thomas-Fermi equation with a convergent approach. Commun Nonlinear Sci Numer Simulat 17: 4097–4103.
24. Zhang W, Qian YH, Lai SK (2012) Extended homotopy analysis method for multi-degree-of-freedom non-autonomous nonlinear dynamical systems and its application. Acta Mech 223: 2537–2548.
25. Sheikholeslami M, Ashorynejad HR, Domairry G, Hashim I (2012) Flow and heat transfer of cu-water nanofluid between a stretching sheet and a porous surface in a rotating system. J Appl Math 2012: 421320.
26. Rashidi MM, Ali M, Freidoonimehr N, Nazari F (2013) Parametric analysis and optimization of entropy generation in unsteady MHD flow over a stretching rotating disk using artificial neural network and particle swarm optimization algorithm. Energy 55: 497–510.
27. Abbasbandy S, Hashemi MS, Hashim I (2013) On convergence of homotopy analysis method and its application to fractional integro-differential equations. Quaestiones Mathematicae 36: 93–105.
28. Hayat T, Naseem A, Farooq M, Alsaedi A (2013) Unsteady MHD three-dimensional flow with viscous dissipation and Joule heating. Europ Phys J Plus 128: 158.
29. Alsaadi FE, Shehzad SA, Hayat T, Monaquel SJ (2013) Soret and Dufour effects on the unsteady mixed convection flow over a stretching surface. J Mech 29: 623–632.
30. Hayat T, Shehzad SA, Al-Mezel S, Alsaedi A (2014) Three-dimensional flow of an Oldroyd-B fluid over a bidirectional stretching surface with prescribed surface temperature and prescribed surface heat flux. J Hydrol Hydromech 62: 117–125.
31. Hayat T, Shehzad SA, Qasim M, Asghar S (2014) Three-dimensional stretched flow via convective boundary conditions and heat generation/absorption. Int J Numer Methods Heat Fluid Flow 24: 342–358.
32. Abbasbandy S, Hayat T, Alsaedi A, Rashidi MM (2014) Numerical and analytical solutions for Falkner-Skan flow of MHD Oldroyd-B fluid. Int J Numer Methods Heat Fluid Flow 24: 390–401.
33. Shehzad SA, Alsaedi A, Hayat T, Alhuthali MS (2013) Three-dimensional flow of an Oldroyd-B fluid with variable thermal conductivity and heat generation/absorption. Plos One 8: e78240.
34. Hayat T, Shehzad SA, Alsaedi A (2013) Three-dimensional stretched flow of Jeffery fluid with variable thermal conductivity and thermal radiation. Appl Math Mech-Eng Edit 34: 823–832.
35. Hayat T, Asad S, Mustafa M, Alsaedi A (2014) Radiation effects on the flow of Powell-Eyring fluid past an unsteady inclined stretching sheet with non-uniform heat source/sink. Plos One 9: e103214.